Accepted refereed manuscript of:

Wan M, Schröder C & Peiffer S (2017) Fe(III):S(-II) Concentration Ratio Controls the Pathway and the Kinetics of Pyrite Formation during Sulfidation of Ferric Hydroxides, *Geochimica et Cosmochimica Acta*, 217, pp. 334-348.

DOI: 10.1016/j.gca.2017.08.036

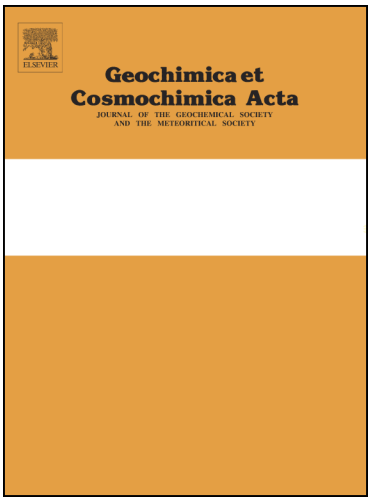

Fe(III):S(-II) Concentration Ratio Controls the Pathway and the Kinetics of Pyrite Formation during Sulfidation of Ferric Hydroxides

Moli Wan, Christian Schröder, Stefan Peiffer

PII: S0016-7037(17)30538-0
DOI: http://dx.doi.org/10.1016/j.gca.2017.08.036
Reference: GCA 10441

To appear in: *Geochimica et Cosmochimica Acta*

Received Date: 5 October 2016

Please cite this article as: Wan, M., Schröder, C., Peiffer, S., Fe(III):S(-II) Concentration Ratio Controls the Pathway and the Kinetics of Pyrite Formation during Sulfidation of Ferric Hydroxides, *Geochimica et Cosmochimica Acta* (2017), doi: http://dx.doi.org/10.1016/j.gca.2017.08.036

Fe(III):S(-II) Concentration Ratio Controls the Pathway and the Kinetics of Pyrite Formation during Sulfidation of Ferric Hydroxides

Moli Wan[1], Christian Schröder[2], Stefan Peiffer[1*]

[1] BayCEER, Department of Hydrology, University of Bayreuth, D-95440, Bayreuth, Germany

[2] Biological and Environmental Sciences, Faculty of Natural Sciences, University of Stirling, Stirling FK9 4LA, Scotland, UK

[*] Corresponding author. Phone ++49-921-552251, Fax ++49-921-552366, s.peiffer@uni-bayreuth.de

Key words

rapid pyrite formation, pathway, polysulfides, reactive ferrous iron, iron-sulfur interaction, ferric hydroxides, Mössbauer spectroscopy

Abstract

The formation of pyrite has been extensively studied because of its abundance in many anoxic environments. Yet, there is no consensus on the underlying pathways and kinetics of its formation. We studied the formation of pyrite during the reaction between reactive ferric hydroxides (goethite and lepidocrocite) and aqueous sulfide in an anoxic glove box at neutral pH. The formation of pyrite was monitored with Mössbauer spectroscopy using ^{57}Fe isotope-enriched ferric (hydr)oxides. The initial molar ratios of Fe(III):S(-II) were adjusted to be 'high' with Fe(III) concentrations in excess of sulfide (HR) and 'low' (LR) with excess of sulfide. Approximately the same surface area was applied in all HR runs in order to compare the mineral reactivity of ferric hydroxides. Electron transfer between aqueous sulfide and ferric hydroxides in the first 2 hours led to the formation of ferrous iron and methanol-extractable oxidized sulfur (MES). Metastable FeS_x formed in all of the experiments. Pyrite formed at a different rate in HR and LR runs although the MES and ferrous iron concentrations were rather similar. In all HR runs, pyrite formation started after 48 hours and achieved a maximum concentration after 1 week. In contrast, pyrite started to form only after 2 months in LR runs (Fe(III):S(-II) ~ 0.2) with goethite and no pyrite formation was observed in LR with lepidocrocite after 6 months. Rates in LR runs were at least 2-3 orders of magnitude slower than in HR runs. Sulfide oxidation rates were higher with lepidocrocite than with goethite, but no influence of the mineral type on pyrite formation rates in HR runs could be observed. Pyrite formation rates in HR runs could not be predicted by the classical model of Rickard (1975). We therefore propose a novel ferric-hydroxide-surface (FHS) pathway for rapid pyrite formation that is based on the formation of a precursor species $>Fe^{II}S_2^-$. Its formation is competitive to FeS_x precipitation at high aqueous sulfide concentrations and requires that a fraction of the ferric hydroxide surface not be covered by a surface precipitate of FeS_x. Hence, pyrite formation rate decreases with decreasing Fe(III):S(-II)$_{aq}$ ratio. In LR runs, pyrite formation appears to follow the model of Rickard (1975) and to be kinetically controlled by the dissolution of FeS. The FHS-pathway will be prominent in many aquatic systems with terrestrial influence, i.e. abundance of ferric iron. We propose that the Fe(III):S(-II)$_{aq}$ ratio can be used as an indicator for rapid pyrite formation during early diagenesis in anoxic/suboxic aquatic systems.

1. Introduction

Sedimentary pyrite formation has been extensively studied because of its abundance in many anoxic environments such as marine and river sediments, groundwater aquifers, and peat lands, and hence its importance in both iron and sulfur cycling. It forms over a wide pH interval, ranging from acidic to alkaline conditions (Luther, 1991; Price and Shieh, 1979; Wilkin and Barnes, 1996). It is generally regarded that sulfide reacting with iron-containing minerals forms metastable iron sulfide minerals before eventually transforming into pyrite in the presence of different sulfur sources (Benning et al., 2000; Berner, 1970; Hellige et al., 2012; Luther, 1991; Rickard, 1997; Rickard and Luther, 1997; Schoonen and Barnes, 1991; Schoonen, 2004). Several studies investigated the transformation from iron sulfide to pyrite, starting with different sulfur species under different conditions. It has been documented that the transformation occurs in solutions containing thiosulfate and zero-valent sulfur such as elemental sulfur and polysulfides (Luther, 1991; Price and Shieh, 1979; Schoonen and Barnes, 1991; Wilkin and Barnes, 1996). In addition, hydrogen sulfide/bisulfide was suggested to sulfidate FeS to form pyrite (Rickard, 1997; Rickard and Luther, 1997; Schoonen, 2004).

A wide spectrum of sulfur species is involved in the transformation of metastable iron sulfide to pyrite, whereby the kinetics and pathways of the transformation appear to be different with different sulfur species. In a homogenous polysulfide solution at neutral pH and ambient temperature, pyrite formation occurred only after 4 months of aging of FeS that precipitated from ferrous iron and aqueous sulfide solution (Luther, 1991). In contrast, solid phase transformation of freeze-dried mackinawite to pyrite under a H_2S atmosphere appeared to occur within 1 day (Rickard, 1997). The rapid formation was later explained in terms of activation of pyrite formation by the occurrence of oxidized sulfur species associated with the dried mackinawite (Benning et al., 2000). Rapid pyrite formation was observed during the interaction between ferric iron and aqueous sulfide/polysulfides, within 2 days under acidic conditions (Berner, 1964; Luther, 1991; Price and Shieh, 1979) and within 14 days at neutral pH (Hellige et al., 2012). In a Transmission Electron Microscopy (TEM) study, Hellige et al. (2012) observed the coating of lepidocrocite crystals by a rim of an amorphous phase rich in Fe and S of localized nano-mackinawite structure after two hours of reaction and complete consumption of aqueous sulfide. The amorphous phase dissolved after several days followed by the precipitation of pyrite nano

phases dislocated from the lepidocrocite surface. In an X-ray photoelectron spectroscopy study performed under comparable experimental conditions, Wan et al. (2014) were able to demonstrate that a large amount of polysulfide species were associated with the ferric (hydr)oxide surface, while aqueous polysulfide species made up only a minor fraction. Of particular importance was disulfide, which - not yet bound as pyrite - seemed to be the main surface polysulfide species. It was suggested that surface polysulfide species, especially surface disulfide, could bind to Fe(II) to form a non-crystalline FeS_2 precursor that triggers the formation of pyrite.

Such experimental observations are matched by field data. In natural sediments with abundant hydrogen sulfide and/or elemental sulfur, metastable iron sulfides dominate with only a minor fraction of pyrite (Burton et al., 2006; Kraal et al., 2013). In contrast, in the fairly oxidized marine sediment of the Santa Catalina Basin, where sulfide concentrations are usually undetectable, pyrite instead of iron monosulfides turns out to be the major mineral in the surface sediments (Kaplan et al., 1963). Rapid pyrite formation (on a time scale of days) has been observed in salt marshes driven by tidal cycling of sulfide (Howarth, 1979; Otero & Macias, 2002).

Previous studies demonstrated that rapid pyrite formation may be linked to excess Fe(II), a fraction of solid-phase Fe(II) formed aside from FeS during sulfidation of ferric hydroxides (Hellige et al., 2012). Formation of excess Fe(II) is proposed to be competitive with respect to FeS precipitation and becomes a significant fraction only in experiments with a high initial ratio of solid Fe(III) to aqueous S(-II) (Fe(III):$S(-II)_{aq}$ ratio, Peiffer et al., 2015). Therefore, in natural systems, a rapid rate of pyrite formation may be observed only under conditions where Fe(III) is in excess to aqueous sulphide. Furthermore, it appears that the rate of pyrite formation upon sulfidation of ferric hydroxides depends on the mineral type (Peiffer et al., 2015). It was proposed that the extent of pyrite formation is ruled by two factors: 1) the ratio between concentrations of added sulfide and available mineral-specific surface area, and 2) the capability of the iron(hydr)oxide to transfer electrons that trigger the formation of pyrite precursor compounds (Peiffer et al., 2015).

In this study we aim to resolve the fate of ferrous iron generated during ferric iron-sulfide interaction and its role on the formation of secondary iron (sulfide) minerals, especially pyrite formation in the presence of different sulfur species such as sulfide and surface and/or aqueous polysulfides. To these ends, ferric hydroxides were reacted with aqueous sulfide at neutral pH in an anoxic glove box at different Fe to S ratios in order to vary the reaction conditions. ^{57}Fe-sensitive Mössbauer spectroscopy was used to analyze the solid phases. Hellige et al (2012) also used Mössbauer spectroscopy but were not able to observe intermediate Fe-S species, only the end product pyrite. They assumed that the intermediate products had been oxidized during sample transport and/or the amount of intermediate was too low to be visible in the Mössbauer spectra. We therefore optimized our measurement procedures by using ^{57}Fe-enriched materials and applying a non-delay measurement.

2. Materials and methods

The experiments were performed in a glove box system (Glovebox system, Innovative Technology, USA) with a working atmosphere of N_2 (99.99%). The oxygen level was in the range of 0-1 ppm. All solutions and organic solvents were purged with N_2 (99.99%) for 1 h to remove oxygen prior to transferring into the glove box. All commercial reagents, except methanol (HPLC grade), were of analytical grade. Sodium sulfide (Na_2S) and methyl trifluoromethanesulfonate (triflate, $CF_3SO_2OCH_3$) were purchased from Sigma-Aldrich, Germany; zinc acetate (ZnAc), iron(II) chloride tetrahydrate ($FeCl_2 \cdot 4H_2O$) and iron(III) nitrate nonahydrate ($Fe(NO_3)_3 \cdot 9H_2O$) from Merck, Germany; methanol (HPLC grade) from Geyer, Germany; and piperazine-N,N′-bis(2-ethanesulfonic acid) (PIPES, $C_8H_{18}N_2O_6S_2$) from VWR , Germany.

2.1 Ferric hydroxides

Synthetic ferric hydroxides were prepared after Schwertmann and Cornell (2008) as previously described in detail by Wan et al. (2014). In brief, to synthesize goethite, 100 mL of a $Fe(NO_3)_3$ solution (c = 1 mol L^{-1}) and 180 mL of a KOH solution (c = 5 mol L^{-1}) were mixed rapidly in a 2 L polyethylene flask. The suspension was diluted to 2 L with distilled water and kept at 70 ℃ for 60 h. To synthesize lepidocrocite, 200 mL of a $FeCl_2$ solution (c = 0.06 mol L^{-1}, pH 6.8) was oxidized by air pumped through the solution at a flow rate of 100 mL min^{-1}. The pH was

maintained at 6.8 by addition of a NaOH solution (c = 0.5 mol L^{-1}) with a pH-stat device (Titrino, Metrohm). The oxidation was carried out at room temperature under gentle continuous stirring. In order to enhance the signal of minor Fe-bearing phases in the Mössbauer spectra, we enriched the ^{57}Fe isotope tenfold in the ferric hydroxides used for Mössbauer analysis. The ^{57}Fe-enriched ferric hydroxides were synthesized according to the same protocol mentioned above, with a modification of reagent preparation: 80 mL of a commercial Fe salt solution ($Fe(NO_3)_2$ and $FeCl_2$) was mixed with 20 mL of corresponding ^{57}Fe salt prior to synthesis. $^{57}Fe(NO_3)_3$ was prepared by dissolution of pure ^{57}Fe metal powder in 20 mL HNO_3 (c = 1 mol L^{-1}) in air. $^{57}Fe(Cl)_2$ was prepared by dissolution of pure ^{57}Fe metal powder in 20 mL hot HCl (c = 2 mol L^{-1}, 60 °C) in the glove box.

The synthetic ferric hydroxides were washed with deionized water (18.2MΩ), freeze dried and characterized by X-ray diffractometry (SIEMENS D-5000 X-ray diffractometer with Co Kα radiation (λ=0.179 nm, cf. Fig S1 and S2). ^{57}Fe-enriched ferric hydroxides were also characterized by Mössbauer spectroscopy, cf. Fig S3 and S4). Both methods identified pure goethite and lepidocrocite, except that ^{57}Fe-enriched lepidocrocite contained 4 % goethite. Multi-point BET (Brunauer, Emmett and Teller) gas adsorption with N_2 (Gemini 2375 analyzer) gave a surface area with 39.33 m^2 g^{-1} for goethite and with 70.24 m^2 g^{-1} for lepidocrocite.

2.2 Experimental set-up

The experiments were performed in a 4-port reactor and followed the set-up described in previous studies (Hellige et al., 2012; Wan et al., 2014). In brief, a 450 mL aqueous sulfide solution (Na_2S) was adjusted to pH 7.0 in the glove box by addition of HCl (c = 1 mol L^{-1}), to which 50 mL of a suspension containing a preselected amount of synthetic ferric hydroxides (goethite or lepidocrocite) was added. The pH was kept constant at pH = 7.0 ± 0.1 with HCl (c= 0.1 mol L^{-1}) using a pH-Stat device with a pH gel electrode without diaphragma to avoid sulfide interferences (Mettler Toledo Inlab Expert). The solution was gently stirred with a Teflon-coated magnetic stirring bar during the whole experiment. The initial conditions of the various experimental runs are listed in Table 1. The sulfide concentration was adjusted prior to the addition of ferric hydroxides, and the total iron concentration was determined after mixing of the sulfide-containing solution with the ferric hydroxides. The initial molar ratios of Fe(III):$S(-II)_{aq}$

were adjusted to be 'high' with Fe concentrations being in excess of sulfide (HR) and 'low' with excess sulfide to Fe in ferric hydroxides (LR). Approximately the same surface-area concentration was used in all HR runs in order to compare the mineral reactivity of ferric hydroxides (Table 1). All runs were conducted at ambient temperature (around 22 ^{o}C) except Runs 8 and 9, which started at ambient temperature and ended at approx. 33^{o}C after 168 h due to an unexpected heating during a warm summer period. A blank experiment running for 168 h in the 4-port reactor with aqueous sulfide at pH 7 yielded a linear H_2S degassing rate of 0.014 mmol L^{-1} h^{-1} (R^2 = 0.914).

In order to prevent degassing of hydrogen sulfide, long-term aging experiments were performed in serum bottles sealed with thick Butyl-septa and aluminium caps through which only trace amounts of sulfide escaped during sampling. The pH was checked regularly and if necessary adjusted by addition of HCl and/or NaOH (c = 0.1 mol L^{-1}). The suspensions were shaken by hand for several minutes every day. The aqueous phase was sampled regularly to determine iron and sulfur speciation and concentrations. Samples for Mössbauer spectroscopy were only taken from the experiments with ^{57}Fe-enriched ferric hydroxides.

Three HR runs were performed with the only purpose to detect proton consumption during the reaction between sulfide and the ferric hydroxides. To this end, H^+ consumption was recorded by the pH-Stat device and no aqueous samples were taken.

Reproducibility of experiments was tested by performing replicate runs under comparable experimental conditions (Pyzik and Sommer, 1981) and statistically analysing 1st order initial rate constants for the formation of Fe(II) and methanol-extractable oxidized sulfur (MES). The analyses could only be performed in HR runs with goethite where the formation of Fe(II) and MES was slow enough to obtain sufficient data. In LR ratio experiments, sampling intervals where much longer than the formation rates so that their evaluation was not possible. For these experiments, we have plotted standard deviations of the mean values from replicate experiments as error bars. In total, 27 experiments were performed where chemical species were analysed (Table 1).

2.2 Sampling and analysis

Wet chemical analysis

Sampling and analytical procedures were performed according to previous studies (Hellige et al., 2012; Wan et al., 2014) with additional evaluation of the effect of low pH on the ferrous iron extraction process. Samples were filtered (0.2 µm, Nylon) and the aqueous phase was analyzed for aqueous ferrous iron ($Fe(II)_{aq}$), aqueous sulfide ($S(-II)_{aq}$), aqueous polysulfide (S_n^{2-}), thiosulfate ($S_2O_3^{2-}$) and sulfate (SO_4^{2-}). Unfiltered samples were analyzed for acid extractable ferrous iron ($Fe(II)_{HCl}$), total iron concentration (Fe_{tot}) and for methanol-extractable sulfur (MES).

Iron species were determined photometrically using the phenanthroline method (Tamura et al., 1974) after specific pre-treatment steps. The total Fe content (Fe_{tot}) was measured at least in triplicate after dissolution of 500 µL of unfiltered samples in 500 µL of hot HCl (c = 12 mol L^{-1}, T = 60 ℃) for 1 week. $Fe(II)_{aq}$ was analyzed after addition of 500 µL HCl (c = 1 mol L^{-1}) into 500 µL filtered samples. $Fe(II)_{HCl}$ was extracted by addition of 500 µL of unfiltered samples into 500 µL of HCl (c = 1 mol L^{-1}) and filtered after 15 min. During the acidic extraction step, metastable iron sulfide (mainly FeS, c.f. eq. 1) will release H_2S, which may generate ferrous iron upon reaction with ferric hydroxides and thus lead to an overestimation of $Fe(II)_{HCl}$ during the acidic extraction. Therefore, test experiments were carried out to quantify the effect of acidic FeS extraction in the presence of ferric hydroxides on the yield of $Fe(II)_{HCl}$. The FeS was precipitated by adding $FeCl_2$ (c = 2 mol L^{-1}) slowly into a Na_2S-containing solution (c = 2 mol L^{-1}). After overnight equilibration, aliquots of the FeS suspension were injected into the ferric (hydr)oxide suspension. Thereafter, HCl (c = 1 mol L^{-1}) was added and allowed to react for 60 min. to extract $Fe(II)_{HCl}$ from the mixture. Samples were taken and filtered after 1 min, 15 min, 30 min and 60 min. Reference runs indicated a complete recovery of $Fe(II)_{HCl}$ after 15 min (103 % ± 6 %). $Fe(II)_{HCl}$ remained constant in the presence of goethite, but increased over time in the presence of lepidocrocite. A mean FeS recovery of 97 % ± 3 % and 119 % ± 4 % was achieved after 15 min in the experiments with goethite and lepidocrocite, respectively. Hence, the $Fe(II)_{HCl}$ seems to be completely recovered in the experiments with goethite, while being overestimated in the presence of lepidocrocite. The $Fe(II)_{HCl}$ concentration was estimated by dividing the measured $Fe(II)_{HCl}$ concentration by the FeS recovery factor (0.97 and 1.19 for goethite and lepidocrocite, respectively). Solid-phase bound Fe(II) ($Fe(II)_{solid}$) (except pyrite-Fe) was then calculated as the difference between the corrected $Fe(II)_{HCl}$ concentration and the measured concentration of

$Fe(II)_{aq}$. $S(-II)_{aq}$ was determined photometrically after filtration and fixation with zinc acetate (ZnAc) (c = 0.1 mol L^{-1}) using the methylene blue method (Fonselius et al., 2007).

SO_4^{2-} was determined turbidimetrically based on the $BaSO_4$ precipitation methods described by Tabatabai (1974). $S_2O_3^{2-}$ was determined by ion-pair chromatography following the methods described by Steudel et al. (1987). Both species were below the detection limit in all runs (detection limits were 6 µmol L^{-1} and 28 µmol L^{-1}, respectively).

Methanol-extractable sulfur (MES) was extracted after pre-treatment of the suspension with ZnAc to precipitate free sulfide, following a procedure modified by Kamyshny et al. (2009). Prior to the extraction step, 250 µL of ZnAc (c = 0.1 mol L^{-1}) were added to 500 µL of the unfiltered sample. After 10 min, 6 mL of methanol were injected into the suspension. The samples were shaken for 3 h and then filtered on 0.2 µm membranes. The filtrates were analyzed for zero-valent sulfur using HPLC as described in Wan et al. (2014). MES comprised all zero-valent sulfur which is in the form of elemental sulfur or associated with aqueous polysulfide (Kamyshny et al., 2009) and surface polysulfide (Wan et al., 2014). The detection limit was below 2 µmol L^{-1} and the standard deviation of the procedure was 1 µmol L^{-1}.

Due to their instability, aqueous polysulfide species were transformed into more stable organic polysulfanes prior to the measurement (Kamyshny et al., 2006, Poser et al, 2013). 200 µL of the filtered samples and 8 µL of triflate were added simultaneously into 1200 µL of methanol previously buffered with 100 µL of phosphate buffer (c = 50 mmol L^{-1}, pH 7) and shaken intensively for 10 s as described in the previous studies (Kamyshny et al., 2006; Wan et al., 2014). The obtained organic polysulfanes were determined with HPLC. The total amount of aqueous polysulfides (S_n^{2-}(aq)) was calculated as the sum of the individual polysulfide fractions (S_2^{2-} (aq) to S_8^{2-} (aq)), as described by Wan et al (2014). The detection limit of this method is reported to be below 1 µmol L^{-1} with the precision of replicates to depend on the chain length of the poylosulfides ranging between between 7 and 32 % (Kamyshny et al, 2006).

The samples for photometric measurements were stored in a dark, cool room (4 ^oC) and measured within one day. The samples for HPLC measurements were stored in a freezer(-18^oC) and measured within one week after preparation.

Mössbauer Spectroscopy

In the experiments with ^{57}Fe-enriched ferric hydroxides, we collected solid phase samples at certain time steps for Mössbauer spectroscopy analysis. The time steps were carefully selected according to our results from wet chemical analysis and the TEM results from Hellige et al. (2012). In the HR runs, samples for high resolution analysis were taken after sulfide was consumed (1.5 h in the experiments with goethite and 15 min with lepidocrocite), after a period when stable transient concentrations were established (3 h with goethite, 2 h with lepidocrocite), during a period when MES decreased (48 h, 72 h with both minerals) and at the end of the experiments (168 h with both minerals). In the LR runs, samples were taken after 72 h and 168 h, and every month thereafter.

To prepare samples of the solid fraction for Mössbauer spectroscopy analysis, 20 mL of the suspension enriched with ^{57}Fe were sampled and filtered through cellulose membrane filter paper (Ø 13 mm and 0.45 μm pore size) inside the glove box until the filter was clogged. The filter and accompanying solid fraction was sealed between two layers of Kapton tape after the small amount of remaining liquid had been carefully removed. The samples were placed in a sealed bottle to avoid contact with air during transportation from the glove box to the spectrometer and measured without further delay. The spectra were collected with a WissEl Mössbauer transmission spectrometer, using a ^{57}Co in Rh matrix γ-ray source mounted on a constant acceleration drive system. Samples were cooled in a Janis closed-cycle Helium gas cryostat that allowed measurements at 140 K, 77 K, 4.2 K as well as room temperature. During measurement, the samples were kept at vacuum or in a low pressure He atmosphere to avoid oxidation. Spectra were calibrated against a spectrum of alpha-Fe(0) foil at room temperature. Data acquisition times were usually about 24 h per spectrum. Spectral fitting was carried out using Recoil software (University of Ottawa, Canada) with the Voigt-based fitting routine. The model parameters for the various ferric minerals are listed in Table 2. The concentration of each iron mineral phase detected by Mössbauer spectroscopy was calculated by multiplying the total Fe concentration (Fe_{tot}) by the respective fitted spectral area representing the relative fraction of individual mineral phases (Supporting Information Table S1).

3. Results

3.1 Chemical speciation

In all runs, consumption of aqueous sulfide ($S(-II)_{aq}$) and built-up of sulfur and ferrous iron species were observed in the first few hours. Following this initial phase, clear differences in the reaction pattern between the various experimental boundary conditions could be observed.

H^+ consumption (concentration of added HCl) was faster in the experiments with lepidocrocite (Fig. 1, run 1 and run 23). H^+ consumption increased initially and achieved a constant level of around 2.2- 2.4 mmol L^{-1} after 2 h in the HR_Gt run, and of around 2.1 mmol L^{-1} after 15 min in the HR_Lp run. We did not record the H^+ consumption after 24 h in the HR_Gt run. In the HR_Lp run, H^+ consumption started to increase steadily after 24 h to 9.6-11.4 mmol L^{-1}.

In the HR runs with goethite (HR_Gt), most of the $S(-II)_{aq}$ was consumed after 1.5 h. The concentration remained lower than 0.05 mmol L^{-1}, then decreased to 0.003 mmol L^{-1} after 24 or 48 h (Fig. 2, run 7 and run 9). Methanol-extractable sulfur (MES) and solid phase bound Fe(II) ($Fe(II)_{solid}$) built up along with the consumption of $S(-II)_{aq}$ in the first 1.5 h, and remained relatively constant for the next several hours. Both species started to decrease after 4 h (run 9) or after 24 h (run 7) with a faster decrease in run 9 at a higher reaction temperature. The concentration of aqueous Fe(II) ($Fe(II)_{aq}$) was around 0.02 mmol L^{-1} in the first 24 h (run 9) or 72 h (run 7) and increased to around 0.5 mmol L^{-1} after 72 h. $S_n^{2-}(aq)$ was detectable only in the first 15 min with a total concentration of 0.03 mmol L^{-1} (data not shown). HR_GT experiments were highly reproducible with 1st order initial rate constants for the formation of total Fe(II) being 3.04 h^{-1} +/- 0.71 h^{-1} (standard deviation, n = 5, runs 3-7) and for MES being 2.55 h^{-1} +/- 0.64 h^{-1} (n=4, runs 4-7).

The reaction in the HR runs with lepidocrocite (HR_Lp) showed a similar pattern but with a faster consumption of $S(-II)_{aq}$ and, correspondingly, a faster built-up of Fe(II) and MES. $S(-II)_{aq}$ was almost completely consumed after 15 min in run 24 (data not shown). In run 25, we started sampling only after 1 h (Fig. 2). $S(-II)_{aq}$ decreased to 0.017 mmol L^{-1} while MES and $Fe(II)_{solid}$ increased to around 2.0 mmol L^{-1} and 6.0 mmol L^{-1} within 1 h and then slowly to 2.2 mmol L^{-1} and 7.0 mmol L^{-1} after 3 h, respectively. After 24 h, the concentration of both species decreased while that of $Fe(II)_{aq}$ started to increase from 0.12 mmol L^{-1} to 0.9 mmol L^{-1} after 168 h. More ferrous iron was generated in the HR_Lp run (run 25) than in the HR_Gt runs (run 7 and run 9). The concentration difference was 1.6 mmol L^{-1} for $Fe(II)_{solid}$ and 0.1 mmol L^{-1} for $Fe(II)_{aq}$ in the

experiments with Lp and Gt, respectively. The difference changed after 168 h to 1.3 mmol L^{-1} for $Fe(II)_{solid}$ and 0.4 mmol L^{-1} for $Fe(II)_{aq}$.

Reproducibility was high also in the LR experiments. Fig. 3B and Fig. 4 display mean values of the concentration of $Fe(II)_{aq}$, $Fe(II)_{solid,}$ MES, $S(-II)_{aq}$ and $S_n^{2-}{}_{(aq)}$ from three or four replicate experiments (Fig. 3B: runs 32-34, Fig 4A: runs 15-18, Fig. 4B: runs 39-42).

In the short-term LR experiments, which ran for 168 h, most of the ferric iron was consumed during the first several hours (Fig. 3). After 3 h, $Fe(II)_{HCl}$ concentrations nearly reached the initial Fe(III) concentrations at 2.9 mmol L^{-1} in the LR run with goethite and 4.2 mmol L^{-1} in the LR runs with lepidocrocite. As the $Fe(II)_{aq}$ concentration remained low, with values ranging between 0.006-0.01 mmol L^{-1} in all of the LR runs, $Fe(II)_{HCl}$ was comprised essentially of solid phase Fe(II) ($Fe(II)_{solid}$). At the same time, MES achieved a concentration of about 1.5 mmol L^{-1} in both LR_Gt and LR_Lp runs. Both species concentrations remained nearly constant thereafter. $S(-II)_{aq}$ decreased after 3 h to 2.3 mmol L^{-1} in the LR_Gt run and to 0.5 mmol L^{-1} in the LR_Lp run, and continued to decrease at a slower rate thereafter. The concentration of S_n^{2-}(aq) rose to 0.5 mmol L^{-1} after 15min and then dropped to 0.03 mmol L^{-1} at the end of the experiments.

In the long-term LR experiments, running for more than 3600 h, and with a higher concentration of inital $S(-II)_{aq}$ (13.9-20.3 mmol L^{-1}), MES, S_n^{2-}(aq) and $Fe(II)_{HCl}$ were the dominant species generated in the presence of a large amount of residual $S(-II)_{aq}$ (>10 mmol L^{-1}, Fig. 4). MES concentrations varied around ~ 1.8 mmol L^{-1} (LR_Gt) and ~1.6 mmol L^{-1} (LR_Lp) with some fluctuation at t = 2800 h. After a short initial increase, the concentration of S_n^{2-}(aq) remained constant at ~0.2 mmol L^{-1} during the entire experiment. $Fe(II)_{aq}$ was not detectable and, thus $Fe(II)_{HCl}$ was comprised of $Fe(II)_{solid}$, the concentration of which remained constant in the presence of both minerals..

In summary, two different reaction patterns were observed. HR runs were quite dynamic within the first 168 h and can therefore be divided into three phases: 1. Consumption of $S(-II)_{aq}$ and build-up of MES and $Fe(II)_{solid}$; 2. Consumption of MES and $Fe(II)_{solid}$; 3. Build-up of an $Fe(II)_{aq}$ pool. In contrast, in LR runs the system seems to reach a steady-state in the presence of high levels of residual aqueous sulfide after the initial consumption of $S(-II)_{aq}$ and formation of MES, $Fe(II)_{solid}$ and S_n^{2-}(aq).

3.2 Mössbauer spectroscopy

We used Mössbauer spectra collected at a sample temperature of ~5 K to identify and quantify Fe-bearing phases in the solid state. At this temperature, the Fe (hydr)oxides are fully magnetically ordered and the resulting six-line subspectra can be easily distinguished from pyrite, which is diamagnetic and displays a two-line subspectrum. Lepidocrocite, in particular, has a magnetic-ordering temperature of 77 K, above which its subspectrum is a paramagnetic two-line pattern with parameters overlapping those of pyrite, making accurate differentiation more difficult.

The Mössbauer spectra revealed the formation of a phase other than Lp, Gt and pyrite in all of the runs shortly after the beginning of the reaction. This phase presents an asymmetric six-line pattern and appears as a minor phase in the HR runs (Fig. 5), and as the dominant or exclusive phase in LR runs (Fig. 6). Spectral fitting excludes greigite. We therefore propose that this phase consists of intermediate Fe-sulfide phases of unknown stoichiometry (i.e. allowing for Fe or S deficiency) that may include mackinawite but not greigite. This attribution is made based on i) TEM observations by Hellige et al. (2012) who reported the presence of a phase rich in Fe and S at the surface of lepidocrocite after a reaction with sulfide; ii) the presence of surface polysulfides and the possibility of Fe-polysulfide association as discussed in Wan et al. (2014); and iii) the fact that the phase appears with consistent Mössbauer parameters throughout our experiments. Mössbauer parameters previously reported for mackinawite (e.g. (Csákberényi-Malasics et al., 2012; Morice et al., 1969; Mullet et al., 2002; Vaughan and Ridout, 1971) are conflicting and are not consistent with any of our results. We are currently trying to resolve this conflict and detailed results will appear in a separate manuscript. In this study, we will refer to this phase as FeS_x with $x \geq 1$ and acknowledge that it may consist of mackinawite as well as other Fe sulfide intermediates.

In HR runs, FeS_x occurred within the first two hours during which no pyrite formation could be observed. After 48 h, pyrite is present in addition to FeS_x. After 168 h, the amount of pyrite had increased significantly while the amount of FeS_x had decreased. It appears that much more Fe(III) of the Lp had reacted to form FeS_x and eventually pyrite. This difference is, however, only

relative and caused by the higher Fe:S ratio (Table 1) in the HR_Gt experiments, which was chosen to compensate for the lower specific surface area of Gt compared to Lp.

In the LR runs with high concentrations of initial $S(II)_{aq}$ (R39 – R42 , $c(S(-II))_{ini}$ =16.5-20.3 mmol L^{-1}), Lp was completely consumed and transformed into FeS_x after 72 h. This phase remained almost unchanged until the end of the experiment, after 3768 h, when still no pyrite formation could be observed (Fig. 6). The major phase in the Gt run was also FeS_x but there are some distinct differences. First, Gt was not completely consumed after 168 h, and a residual amount of Gt remained until the end of the experiment after 3672 h. Secondly, pyrite had formed after 2880 h.

4. Discussion

4.1 Kinetics of pyrite formation

The formation of pyrite during interaction between ferric iron and sulfide was observed in several studies (Hellige et al., 2012; Price and Shieh, 1979). Elemental sulfur, polysulfides (mainly associated with the surface) and solid-phase ferrous iron species are key initial products (Hellige et al., 2012; Price and Shieh, 1979; Wan et al., 2014) essential for pyrite formation (Luther, 1991; Rickard and Morse, 2005; Rickard, 1975; Schoonen and Barnes, 1991; Schoonen, 2004; Wilkin and Barnes, 1996). In our study, MES (oxidized sulfur comprising elemental sulfur, surface-bound polysulfides and traces of aqueous polysulfides) as well as $Fe(II)_{HCl}$ reached their maximum concentrations (1-2.5 mmol L^{-1} and 4-7 mmol L^{-1}, respectively) within 3 h after completion of sulfide oxidation in both HR and LR runs (Fig. 2 and Fig. 3). Concentrations of $S(-II)_{aq}$ were in the micro-molar range in HR runs and in the milli-molar range in LR runs. Although the concentrations of MES and ferrous iron in LR runs were similar to those in HR runs (between 1-2.5, and 2.9-7 mmol L^{-1} for MES and ferrous iron, respectively), pyrite formation was significantly faster in HR runs than in LR runs (Fig. 7). MB spectra indicate that, in HR runs, the onset of pyrite formation is accompanied by a decrease in MES and ferrous iron concentrations after 24-48 h (Fig. 2).

We can now examine whether the observed pyrite formation can be predicted with the classic polysulfide model that describes pyrite formation in a suspension containing elemental sulfur,

aqueous sulfide and FeS (Rickard, 1975). In such systems, polysulfides form rapidly during the reaction between elemental sulfur and aqueous sulfide (eq 1a) (Kamyshny et al., 2006).

$$HS^- + \frac{n-1}{8} S_8 = H^+ + S_n^{2-} \quad (1a)$$

Polysulfides then react further with FeS to form pyrite (eq. 1b)

$$FeS + S_n^{2-} = FeS_{2,py} + S_{n-1}^{2-} \quad (1b)$$

In this model, the rate of pyrite formation is regarded to be second order with respect to the surface area of FeS and of first order with respect to the surface area of elemental sulfur and the activities of aqueous sulfide species and hydrogen ions (Rickard, 1975, eq 2).

$$R = k \,.\, (A_{FeS})^2 \,.\, A_{S^0} \,.\, a_{s(-II)_{aq}} \,.\, a_{H^+} \quad (2)$$

where R denotes the pyrite formation rate [mol L^{-1} s^{-1}]; A_{FeS} and A_{S^o} are the surface areas of FeS and of elemental sulfur [cm^2], respectively; $a_{s(-II)_{aq}}$ is the sum of activities of aqueous sulfide species as derived from equilibrium calculations at a constant partial pressure of H_2S, and a_{H^+} denotes the hydrogen ion activity.

A numerical value for *k* at 20 °C of 1.5×10^{-13} cm^6 mol^{-1} L^{-1} s^{-1} is provided by Rickard (1975). However, a closer inspection of this value revealed it to be erroneous because of the incorrect use of units in the original publication. We have therefore recalculated the rate constant to be 1.2×10^4 L^4 mol^{-4} s^{-1} using the original data from Rickard (1975) and converting surface areas into concentrations (eq 3) (detailed calculation process c.f. appendix).

$$R = k \,.\, (c_{FeS})^2 \,.\, c_{S^0} \,.\, c_{S(-II)_{aq}} \,.\, c_{H^+} \quad (3)$$

Neglecting ionic strength effects, the above equation can be rewritten as

$$R = k' \,.\, (c_{FeS})^2 . c_{S^0} \quad (4)$$

where

where $k' = k . c_{S(-II)_{aq}} . c_{H^+}$

Equation (4) can be integrated to obtain a relationship between pyrite concentration and reaction time (detailed integration procedure c.f. appendix)

$$t = \frac{1}{k'} . \left[\frac{1}{(B-A)^2} . \ln \frac{(A-y)}{(B-y)} + \frac{1}{(B-A).(A-y)} + \left(\frac{1}{A.(A-B)} - \frac{1}{(B-A)^2} . \ln \frac{A}{B} \right) \right] \qquad (5)$$

where A and B denote initial concentrations of FeS and S^o [mol L-1], respectively. y (y < A and y < B) [mol L^{-1}] is the concentration of generated pyrite and t [s] is the reaction time.

In order to test whether the integrated form of the Rickard model is able to predict pyrite formation within the experimental time scales of this study (Figs 2, 3 and 4), equation (5) was solved for the following conditions.

The pH in our experiments was constant. After the sulfidation step of the ferric hydroxides (first phase), the concentrations of $S(-II)_{aq}$ remained in a range of 10^{-5} mol L^{-1} and 10^{-2} mol L^{-1} in HR and LR runs, respectively. As a best and conservative guess, we assumed the $S(-II)_{aq}$ concentrations to remain constant in both HR and LR runs.

For simplicity, we approximated the concentrations of S^o and FeS by the measured peak concentrations of MES and $Fe(II)_{HCl}$, respectively, after 3 h, i.e. 2.5 mmol L^{-1} MES and 7 mmol L^{-1} $Fe(II)_{HCl}$ for the HR runs, and 2 mmol L^{-1}MES and 4 mmol L^{-1} $Fe(II)_{HCl}$ for the LR runs. Hence, application of equation (5) provides a maximum estimate of pyrite formation rates since reactants did not remain constant, particularly in the HR runs.

Predicted pyrite concentrations after 3900-4100h (comparable to our LR experiments) were negligible (10^{-10} and 10^{-8} mol L^{-1}) (Fig. 7). Only in the LR_Lp run did the pyrite formation rate match the model. All other experiments, HR_Lp, HR_Gt and LR_Gt generated significantly more pyrite. In particularly, pyrite formation rates in HR runs are orders of magnitude faster than predicted by the Rickard model.

Overall, this assessment demonstrates that the Rickard model cannot be applied to pyrite formation at least at high initial molar ratios of Fe(III) to $S(-II)_{aq}$.

4.2 The role of surface associated S and Fe species in pyrite formation

Since Rickard's model (1975) cannot satisfactorily explain the kinetics of pyrite formation in our experiments, we propose that pyrite can nucleate and grow in the presence of ferrous iron and disulfide species.

The rate-limiting processes for pyrite nucleation and/or crystal growth are regarded to be the production of reactive sulfur species and of reactive ferrous iron (Luther, 1991; Rickard, 2012; Schoonen and Barnes, 1991). It was demonstrated that, in the presence of both ferrous iron and disulfide/polysulfides, pyrite formation is kinetically controlled by the degree of supersaturation with respect to pyrite Ω_{py}-1 (eq. 6)

$$\Omega_{py} - 1 = \frac{\{Fe^{2+}\}.\{S_2^{2-}\}}{K_{sp}} - 1 \qquad (6)$$

where brackets denote the activities of the corresponding ions and K_{sp} is the thermodynamic solubility product of pyrite (8.5×10^{-26}, Harmandas et al., 1998). Achievement of a critical supersaturation readily initiates spontaneous pyrite nucleation (Harmandas et al., 1998; Rickard, 2012; Schoonen and Barnes, 1991). Hence, the question arises as to whether the two experimental approaches (HR vs. LR runs) differ in their supersaturation degree and this difference may provide an explanation for the observed differences in pyrite formation rates. We have therefore estimated the maximum values for the degree of supersaturation for the contrasting experimental conditions in the HR and LR runs, based on measured reactant concentrations or reasonable estimates.

It is generally assumed that only aqueous species contribute to pyrite nucleation. In HR experiments, $Fe(II)_{aq}$ is detectable, but concentrations of $S_n^{2-}(aq)$ (including $S_2^{2-}(aq)$) are below the detection limit. Nevertheless, the occurrence of surface bound polysulfides, as observed by Wan et al. (2014), makes the formation of $S_n^{2-}(aq)$ and/or $S_2^{2-}(aq)$ likely upon equilibration with the aqueous phase. As a maximum estimate, we assume the $S_2^{2-}(aq)$ concentration to be 1µmol L^{-1} in HR runs, i.e. in the range of the analytical detection limit. In LR runs, the total $S_n^{2-}(aq)$ concentration was around 0.2 mmol L^{-1} which we are using as a maximum estimate for the $S_2^{2}(aq)$ concentration in these experiments. Fe(II) concentrations were below the detection limit so that we used a value of 1 µmol L^{-1} as a maximum estimate for the Fe(II) concentration. At neutral pH, $Fe(II)_{aq}$ concentration appears to be independent of sulfide concentration and to be in the range of 1 µmol L^{-1} in the presence of dissolved sulphide (Rickard, 2006).

With these maximum estimates for the reactant concentrations of each run, calculated degrees of supersaturation were very similar between HR and LR runs and ranged between $1.3 \cdot 10^{14}$ and $2.3 \cdot 10^{15}$ (Table 3). These maximum estimates approximately match the degree of supersaturation of

$5.7 \cdot 10^{14}$ (± 10 %) that was regarded to be the limit at which solutions supersaturated with respect to pyrite remain stable (Harmandas et al., 1998). Irrespective of the validity of this threshold, even after several months, these estimates would predict similar pyrite precipitation behaviour in HR and LR runs. Such prediction, however, conflicts with the observed pyrite formation rates that are up to 3 orders of magnitude higher in HR runs than in LR runs (Fig. 7). We therefore conclude that other species are involved in pyrite nucleation in HR runs. As was demonstrated in companion experiments, polysulfide species are associated with the mineral surface and their concentration is high. Wan et al (2014) observed that up to 100 % of the oxidized sulfur consisted of polysulfides bound to the mineral surface (S_n^{2-}(surf)). Analytically, S_n^{2-}(surf) species made up most the oxidized sulfur detected as MES so that MES can be used as a proxy for surface polysulfide species. The fraction of surface-bound disulfide (S_2^{2-}(surf)) ranged between 20% - 34% of the measured MES concentration (Wan et al., 2014).

Measured MES concentrations in HR runs, however, are only slightly higher than those in LR runs (< 1mmol L^{-1}). We therefore conclude that the concentrations of S_n^{2-}(surf) are not very different between the experiments. MES concentrations measured after 3 h in HR runs of this study were 2.0-2.5 mmol L^{-1} and 1.8-2.0 mmol L^{-1} in LR runs, respectively. Taking the mean values from all measurements, we obtain a rough estimate for the concentration of S_2^{2-}(surf) to be 0.6 mmol L^{-1} in HR runs and 0.5 mmol L^{-1} in LR runs, respectively. Hence, the occurrence of these species does not provide an explanation for the observed higher pyrite formation rates in HR runs.

4.3 A novel pathway for pyrite formation

Metastable iron monosulfide (FeS) has been suggested as a precursor for pyrite formation in supplying $Fe(II)_{aq}$ (Luther, 1991; Schoonen and Barnes, 1991), but $Fe(II)_{aq}$ does not necessarily need to be generated by the dissolution of FeS. Any iron compound capable of supplying $Fe(II)_{aq}$ can potentially contribute to pyrite formation (Rickard, 2012). Interestingly, significant amounts of HCl-extractable Fe(II) were identified in previous studies (Hellige et al., 2012; Poulton, 2003; Poulton et al., 2004) that appeared not to be bound to FeS (excess Fe(II) (Hellige et al., 2012)).

Below, we will re-examine Fe(II) generation during the interaction between aqueous sulfide and ferric hydroxides. Instead of FeS, we will apply the term FeS_x to account for the results from

Mössbauer spectroscopy (Figs. 5 and 6). A reaction sequence has been proposed according to which, after a series of surface complexation reactions (eq 7a), electron transfer (eq 7b), and reactive sulfur radical release (eq 7c), a surface species ($>Fe^{II}OH_2^+$) forms that could release Fe^{2+} (eq 7d) (Dos Santos Afonso and Stumm, 1992).

$$>Fe^{III}OH + HS^- \leftrightarrow >Fe^{III}S^- + H_2O \quad (7a)$$

$$>Fe^{III}S^- \leftrightarrow >Fe^{II}S^\bullet \quad (7b)$$

$$>Fe^{II}S^\bullet + H_2O \leftrightarrow >Fe^{II}OH_2^+ + S^{\bullet-} \quad (7c)$$

$$>Fe^{II}OH_2^+ \xrightarrow{H^+} new\ surface\ site + Fe^{2+} \quad (7d)$$

Fe^{2+} can be trapped by FeS_x precipitation in the presence of aqueous sulfide, the rate of which is believed to be limited by the steps summarized in reactions 7a – 7d (Pyzik and Sommer, 1981). FeS formation was observed in most of the studies that investigated pyrite formation (Benning et al., 2000; Hellige et al., 2012; Luther, 1991; Poulton, 2003; Price and Shieh, 1979; Schoonen and Barnes, 1991; Schoonen, 2004) as well as in this study. However, when establishing an electron balance, several studies have demonstrated that a substantial fraction of the generated Fe(II) could not be attributed to FeS_x in experiments with a high Fe(III) to $S(-II)_{aq}$ concentration ratio (analogously to our HR runs). This fraction was referred to as 'surface bound Fe(II)' in Poulton et al. (2004) or 'excess Fe(II)' in Hellige et al. (2012). It was proposed that this excess Fe(II) is associated with the surface (Hellige et al., 2012; Poulton, 2003; Poulton et al., 2004) or consists of electron equivalents stored in the surface layers of the bulk mineral (Peiffer and Wan, 2016).

In a previous study (Peiffer et al., 2015), a kinetic model was proposed according to which the competition between excess Fe(II) and FeS_x formation is ruled by two factors: 1) the concentration ratio between the dissolved sulfide added and the available surface area of the ferric hydroxides, and 2) the capability of the iron(hydr)oxide to conduct electrons from surface bound $>Fe^{II}OH_2^+$ to bulk Fe(III) and to accommodate structural Fe(II) which depends on the kinetics of electron transfer between $>Fe^{II}OH_2^+$ and the properties of the bulk mineral. With increasing initial sulfide concentration, precipitation of FeS would become kinetically favoured. The concentration of $>Fe^{II}OH_2^+$ decreases upon precipitation of FeS_x and is fully consumed when

sulfide is in large excess to ferric hydroxides, which is the case in our LR runs with a initial molar Fe(III):$S(-II)_{aq}$ ratios < 0.2.

In HR runs, oxidation of sulfide (eq 7b) reduces the amount of aqueous sulfide available to trap $>Fe^{II}OH_2^+$ and to precipitate FeS_x, whereas in LR runs the pool of aqueous sulfide remains high. The generated $>Fe^{II}OH_2^+$ may possibly induce electron transfer with the bulk ferric host mineral (Peiffer et al., 2015) as well as trigger the formation of secondary minerals such as magnetite (Hellige et al., 2012).

The species $>Fe^{II}OH_2^+$ may also react with the recombined sulfide radical $S^{\bullet-}$ to generate a surface species such as $>Fe^{II}S_2^-$

$$> Fe^{II}OH_2^+ + 2S^{\cdot-} \rightarrow H_2O + > Fe^{II}S_2^- \qquad (8)$$

or with even longer S chains.

The reaction is competive with FeS_x formation and therefore the probability of $>Fe^{II}S_2^-$ and/or $>Fe^{II}S_n^-$ (n>2) formation decreases with an increase in initial sulfide concentration. In the presence of high sulfide concentrations (i.e. in LR runs), the formation of $>Fe^{II}S_2^-$ and/or $>Fe^{II}S_n^-$ (n>2) is unfavourable.

We propose that $>Fe^{II}S_2^-$ may trigger rapid pyrite nucleation through a dynamic equilibrium with the aqueous phase (eq 9)

$$> Fe^{II}S_2^- \overset{H^+}{\rightarrow} FeS_{2,aq} + new\ surface\ site \qquad (9)$$

and subsequent nucleation of FeS_2. According to this model, $>Fe^{II}S_2^-$ would act as a pyrite precursor species that decreases the required degree of supersaturation for pyrite nucleation and allows for the observed rapid pyrite formation.

This model is difficult to test with our current knowledge about the occurrence of the postulated $>Fe^{II}S_2$ species. Neither Mössbauer spectroscopy nor XPS would provide information about such a surface complex and future studies should focus on the fine structure of Fe-S bonding at the mineral surface. The most prominent feature of runs where pyrite formation was observed is the occurrence of large fractions of residual Fe(III) in HR runs with high pyrite formation rates and, to a much lower extent, also in those LR runs where at least some pyrite

formation was observed (cf. Fig. 6). It therefore remains to be investigated whether the postulated pyrite formation pathway requires that a fraction of the ferric hydroxide surface not be covered by a surface precipitate of FeS_x.

5. Conclusion and Implication

Results of this study imply an alternative pathway for pyrite formation when ferric iron concentration is in excess of aqueous sulfide, which we propose to refer to as the ferric-hydroxide-surface (FHS) pathway. The key species controlling the overall pyrite formation mechanism appears to be $>Fe^{II}OH_2^+$, i.e. ferrous iron forming at the mineral surface upon sulfidation of ferric hydroxides. When the FHS-pathway dominates, sulfide concentrations are maintained upon reaction with ferric (hydr)oxides at a level that does not allow for complete sequestration of the $>Fe^{II}OH_2^+$ as FeS. Such conditions give rise to interaction of $>Fe^{II}OH_2^+$ with polysulfide species that triggers the formation of the pyrite precursor species $>FeS_2^-$ and allows for rapid pyrite formation. In contrast, when aqueous sulfide is in excess to Fe(III), the generated Fe(II) is trapped by $S(-II)_{aq}$ to precipitate as FeS. Pyrite formation under these conditions is kinetically controlled by the attainment of a critical supersaturation from dissolution of FeS.

We propose to use the $Fe(III):S(-II)_{aq}$ concentration ratio as a proxy for the pyrite formation pathway in anaerobic/suboxic systems. For example, a re-flooded, freshwater wetland system characterized by the absence of FeS and the abundance of pyrite has been described by Johnston et al. (2014). The pore water was depleted in aqueous sulfide but contained high concentrations of aqueous ferrous iron as well as reactive ferric iron in the near-surface sediments. The $Fe(III):S(-II)_{aq}$ concentration ratio in this system is high and results of our study would imply that the FHS-pathway is active under these conditions. A system with a low $Fe(III):S(-II)_{aq}$ concentration ratio has been discussed by (Kraal et al., 2013). In this case, ferrous iron was depleted in the pore water, rapid pyrite formation was not favourable and FeS was usually preserved and dominated in the near-surface sediments.

Generally, freshwater systems or marine systems with terrestrial influence, which are rich in ferric iron, would be candidates for the FHS-pathway. Recent studies have demonstrated a cryptic or hidden sulfur cycle in low-sulfate environments where rapid reoxidation of sulfide presumably occurs at the surface of ferric (hydr)oxides (e. g. Pester et al, 2012, Holmkvist et al, 2011, Hansel

et al, 2015). Hence, steady-state sulfide concentrations rarely exceed 20 μmol L^{-1} in such systems (e. g. Howarth, 1979; Otero and Macias, 2002, Giblin and Howarth, 1984; Giblin, 1988) and pyrite formation is rapid (on a time scale of days).

Experiments in this and other studies (e. g. Yao and Millero, 1996; Poulton et al, 2004) have been performed under conditions where the initial amount of S(-II) was added as a pulse (e. g. 10 mmol L^{-1}) to a suspension of excess ferric oxides. Fe(III) – S(-II) interactions under steady but low S(-II) supply conditions have never been studied so far. It can be expected that the precipitation of FeS under these conditions, other than in pulse experiments, is not possible and that the mean oxidation state of the reacted sulfur is even higher than observed in this and previous studies with an even higher yield and rate of pyrite formation.

Acknowledgements

This research was funded by the Helmholtz Wasser-Allianz and the Deutsche Forschungsgemeinschaft (DFG) through DFG Research Unit 580 “Electron Transfer Processes in Anoxic Aquifers” (PE 438/12-1,2,3). We thank Stefan Haderlein and Andreas Kappler, University of Tübingen for our use of their Mössbauer spectrometer. We also thank the staff members of the Department of Hydrology, University of Bayreuth for help and support as well as the asscociate editor A. Mucci and three anonymous reviewers for their valuable comments.

Benning, L.G., Wilkin, R.T. and Barnes, H. (2000) Reaction pathways in the Fe–S system below 100 C. Chemical Geology 167, 25-51.
Berner, R.A. (1964) Iron sulfides formed from aqueous solution at low temperatures and atmospheric pressure. The Journal of Geology, 293-306.
Berner, R.A. (1970) Sedimentary pyrite formation. American Journal of Science 268, 1-23.
Burton, E.D., Bush, R.T. and Sullivan, L.A. (2006) Sedimentary iron geochemistry in acidic waterways associated with coastal lowland acid sulfate soils. Geochimica et Cosmochimica Acta 70, 5455-5468.
Csákberényi-Malasics, D., Rodriguez-Blanco, J.D., Kis, V.K., Rečnik, A., Benning, L.G. and Pósfai, M. (2012) Structural properties and transformations of precipitated FeS. Chemical Geology 294, 249-258.
Dos Santos Afonso, M. and Stumm, W. (1992) Reductive dissolution of iron(III) (hydr)oxides by hydrogen sulfide. Langmuir 8, 1671-1675.
Fonselius, S., Dyrssen, D. and Yhlen, B. (2007) Determination of hydrogen sulphide. Methods of Seawater Analysis, Third Edition, 91-100.
Giblin, A.E. (1988) Pyrite formation in marshes during early diagenesis. Geomicrobiology Journal 6, 77-97.

Giblin, A.E. and Howarth, R.W. (1984) Porewater evidence for a dynamic sedimentary iron cycle in salt marshes. Limnol. Oceanogr 29, 47-63.
Hansel, C.M., Lentini, C.J., Tang, Y., Johnston, D.T., Wankel, S.D. and Jardine, P.M. (2015) Dominance of sulfur-fueled iron oxide reduction in low-sulfate freshwater sediments. The ISME journal 9, 2400-2412.
Harmandas, N.G., Navarro Fernandez, E. and Koutsoukos, P.G. (1998) Crystal Growth of Pyrite in Aqueous Solutions. Inhibition by Organophosphorus Compounds. Langmuir 14, 1250-1255.
Hellige, K., Pollok, K., Larese-Casanova, P., Behrends, T. and Peiffer, S. (2012) Pathways of ferrous iron mineral formation upon sulfidation of lepidocrocite surfaces. Geochimica et Cosmochimica Acta 81, 69-81.
Holmkvist, L., Ferdelman, T.G. and Jørgensen, B.B. (2011) A cryptic sulfur cycle driven by iron in the methane zone of marine sediment (Aarhus Bay, Denmark). Geochimica et Cosmochimica Acta 75, 3581-3599.
Howarth, R.W. (1979) Pyrite: its rapid formation in a salt marsh and its importance in ecosystem metabolism. Science 203, 49-51.
Johnston, S.G., Burton, E.D., Aaso, T. and Tuckerman, G. (2014) Sulfur, iron and carbon cycling following hydrological restoration of acidic freshwater wetlands. Chemical Geology 371, 9-26.
Kamyshny, A., Borkenstein, C.G. and Ferdelman, T.G. (2009) Protocol for Quantitative Detection of Elemental Sulfur and Polysulfide Zero-Valent Sulfur Distribution in Natural Aquatic Samples. Geostandards and Geoanalytical Research 33, 415-435.
Kamyshny, A., Ekeltchik, I., Gun, J. and Lev, O. (2006) Method for the determination of inorganic polysulfide distribution in aquatic systems. Analytical Chemistry 78, 2631-2639.
Kaplan, I.R., Emery, K.O. and Rittenbebg, S.C. (1963) The distribution and isotopic abundance of sulphur in recent marine sediments off southern California. Geochimica et Cosmochimica Acta 27, 297-331.
Kraal, P., Burton, E.D. and Bush, R.T. (2013) Iron monosulfide accumulation and pyrite formation in eutrophic estuarine sediments. Geochimica et Cosmochimica Acta 122, 75-88.
Luther, G.W. (1991) Pyrite synthesis via polysulfide compounds. Geochimica et Cosmochimica Acta, 2839-2849.
Morice, J., Rees, L. and Rickard, D. (1969) Mössbauer studies of iron sulphides. Journal of Inorganic and Nuclear Chemistry 31, 3797-3802.
Mullet, M., Boursiquot, S., Abdelmoula, M., Génin, J.-M. and Ehrhardt, J.-J. (2002) Surface chemistry and structural properties of mackinawite prepared by reaction of sulfide ions with metallic iron. Geochimica et Cosmochimica Acta 66, 829-836.
Otero, X.L. and Macias, F. (2002) Variation with depth and season in metal sulfides in salt marsh soils. Biogeochemistry 61, 247-268.
Peiffer, S., Behrends, T., Hellige, K., Larese-Casanova, P., Wan, M. and Pollok, K. (2015) Pyrite formation and mineral transformation pathways upon sulfidation of ferric hydroxides depend on mineral type and sulphide concentration. Chemical Geology 400, 44-55.
Peiffer, S. and Wan, M. (2016) Reductive Dissolution and Reactivity of Ferric (Hydr) oxides: New Insights and Implications for Environmental Redox Processes. Iron Oxides: From Nature to Applications, 31-52.
Pester, M., Knorr, K.-H., Friedrich, M.W., Wagner, M. and Loy, A. (2012) Sulfate-reducing microorganisms in wetlands–fameless actors in carbon cycling and climate change. Front Microbiol, 3, 72.
Poser, A., Lohmayer, R., Vogt, C., Knoeller, K., Planer-Friedrich, B., Sorokin, D.,Richnow, H., Finster, K. (2013) Disproportionation of elemental sulfur by haloalkaliphilic bacteria from soda lakes. Extremophiles, 17, 1003-1012
Poulton, S.W. (2003) Sulfide oxidation and iron dissolution kinetics during the reaction of dissolved sulfide with ferrihydrite. Chemical Geology 202, 79-94.

Poulton, S.W., Krom, M.D. and Raiswell, R. (2004) A revised scheme for the reactivity of iron (oxyhydr)oxide minerals towards dissolved sulfide. Geochimica et Cosmochimica Acta 68, 3703-3715.
Price, F.T. and Shieh, Y. (1979) Fractionation of sulfur isotopes during laboratory synthesis of pyrite at low temperatures. Chemical Geology 27, 245-253.
Pyzik, A. J. and Sommer, S. E. (1981) Sedimentary iron monosulfides: kinetics and mechanism of formation. Geochimica et Cosmochimica Acta 45, 687-698
Rickard, D. (1997) Kinetics of pyrite formation by the H2S oxidation of iron(II) monosulfide in aqueous solutions between 25-125 °C: the rate equation. Geochimica et Cosmochimica Acta 61, 115-134.
Rickard, D. (2006) The solubility of FeS. Geochimica et Cosmochimica Acta 70, 5779-5789.
Rickard, D. (2012) Sulfidic sediments and sedimentary rocks. Elsevier, Amsterdam.
Rickard, D. and Luther, G.W. (1997) Kinetics of pyrite formation by the H2S oxidation of iron (II) monosulfide in aqueous solutions between 25 and 125 °C: The mechanism. Geochimica et Cosmochimica Acta 61, 135-147.
Rickard, D. and Morse, J.W. (2005) Acid volatile sulfide (AVS). Marine Chemistry 97, 141-197.
Rickard, D.T. (1975) Kinetics and mechanism of pyrite formation at low temperatures. American Journal of Science 275, 636-652.
Schoonen, M. and Barnes, H. (1991) Reactions forming pyrite and marcasite from solution: II. Via FeS precursors below 100 C. Geochimica et Cosmochimica Acta 55, 1505-1514.
Schoonen, M.A. (2004) Mechanisms of sedimentary pyrite formation. SPECIAL PAPERS-GEOLOGICAL SOCIETY OF AMERICA, 117-134.
Schwertmann, U. and Cornell, R.M. (2008) Iron oxides in the laboratory. Wiley-Vch.
Steudel, R., Holdt, G., Göbel, T. and Hazeu, W. (1987) Chromatographic Separation of Higher Polythionates SnO 62-(n= 3… 22) and Their Detection in Cultures of Thiobacillus ferroxidans; Molecular Composition of Bacterial Sulfur Secretions. Angewandte Chemie International Edition in English 26, 151-153.
Tabatabai, M. (1974) A rapid method for determination of sulfate in water samples. Environmental Letters 7, 237-243.
Tamura, H., Goto, K., Yotsuyanagi, T. and Nagayama, M. (1974) Spectrophotometric determination of iron (II) with 1, 10-phenanthroline in the presence of large amounts of iron (III). Talanta 21, 314-318.
Vaughan, D. and Ridout, M. (1971) Mössbauer studies of some sulphide minerals. Journal of Inorganic and Nuclear Chemistry 33, 741-746.
Wan, M., Shchukarev, A., Lohmayer, R., Planer-Friedrich, B. and Peiffer, S. (2014) Occurrence of Surface Polysulfides during the Interaction between Ferric (Hydr)Oxides and Aqueous Sulfide. Environmental Science & Technology 48, 5076-5084.
Wilkin, R. and Barnes, H. (1996) Pyrite formation by reactions of iron monosulfides with dissolved inorganic and organic sulfur species. Geochimica et Cosmochimica Acta 60, 4167-4179.

List of Figures

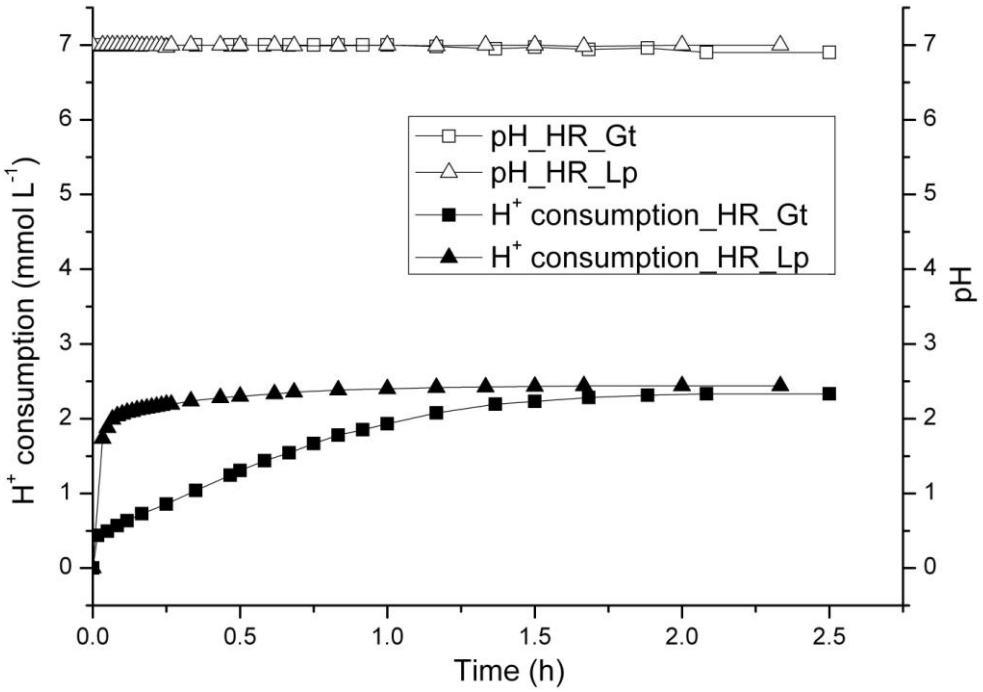

Fig. 1 pH value and H^+ consumption within the first 2.5 h of two HR runs (run 1 and 23) with goethite and lepidocrocite

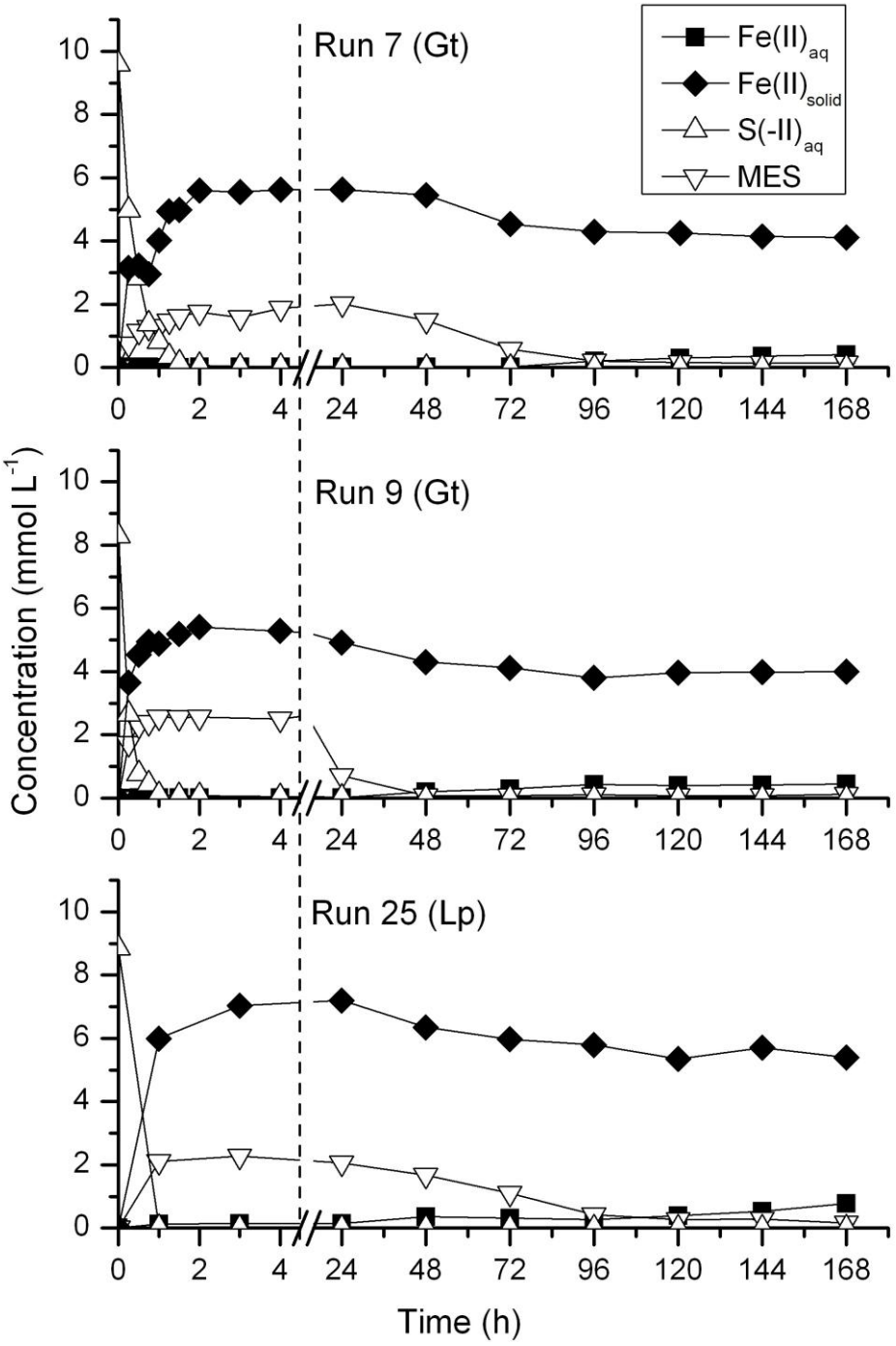

Fig. 2 Temporal changes of iron and sulfur species concentrations in three HR runs

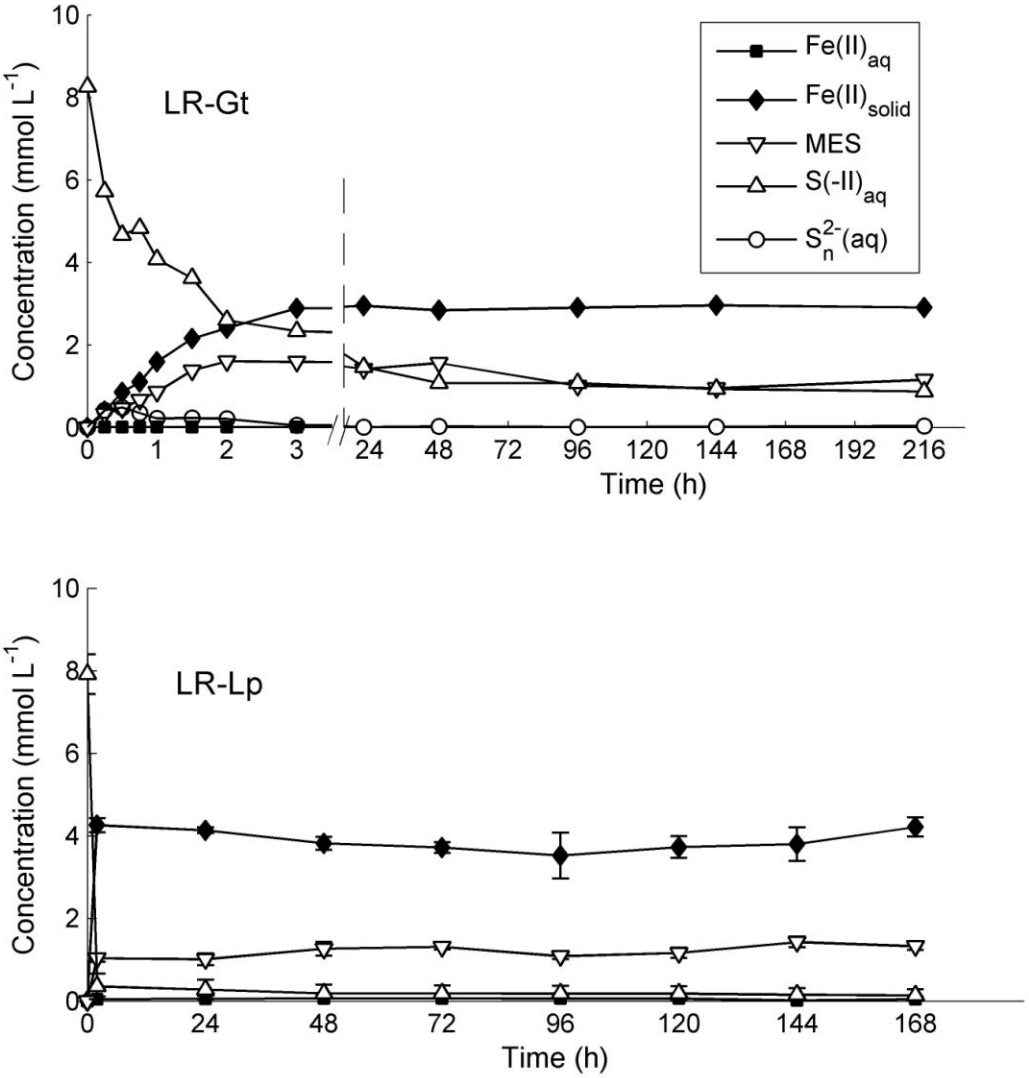

Fig. 3 Temporal changes of iron and sulfur species concentrations in the short-term LR runs (168 h), Fig 3 A (LR-Gt): run 14, Fig. 3B (LR-Lp): runs 32-34. Error bars in Figure 3A denote standard deviations around the mean value from three replicate experiments.

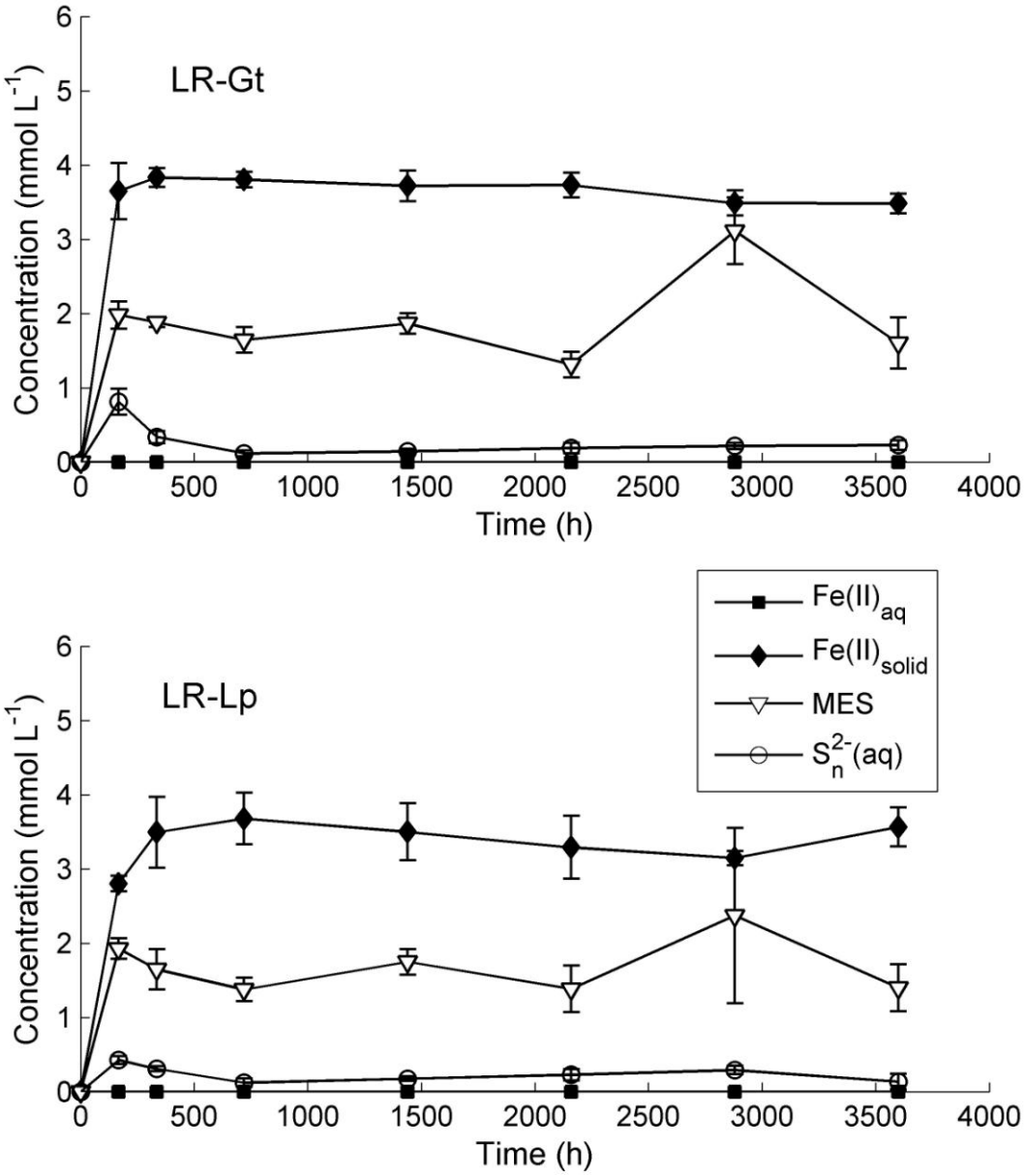

Fig. 4 Temporal changes of iron and sulfur species concentrations in the long-term LR runs (3600 h), Fig 4 A (LR-Gt): runs 15-18, Fig. 4B (LR-Lp): runs 39-42. Error bars denote standard deviations around the mean value from four replicate experiments.

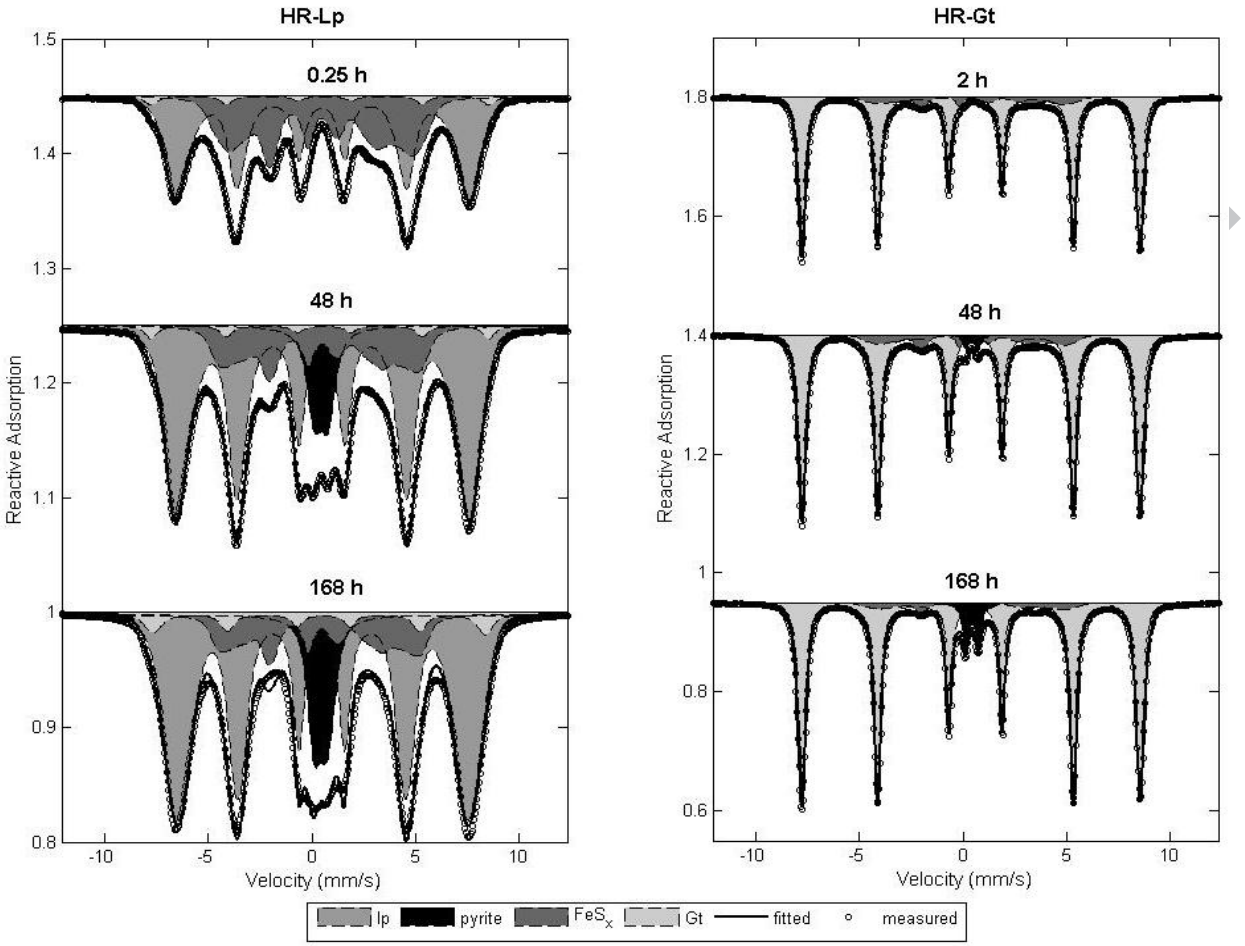

Fig. 5 Mössbauer spectra taken during two HR runs (run 28 and 10). The model parameters used for spectra fitting are listed in Table 2.

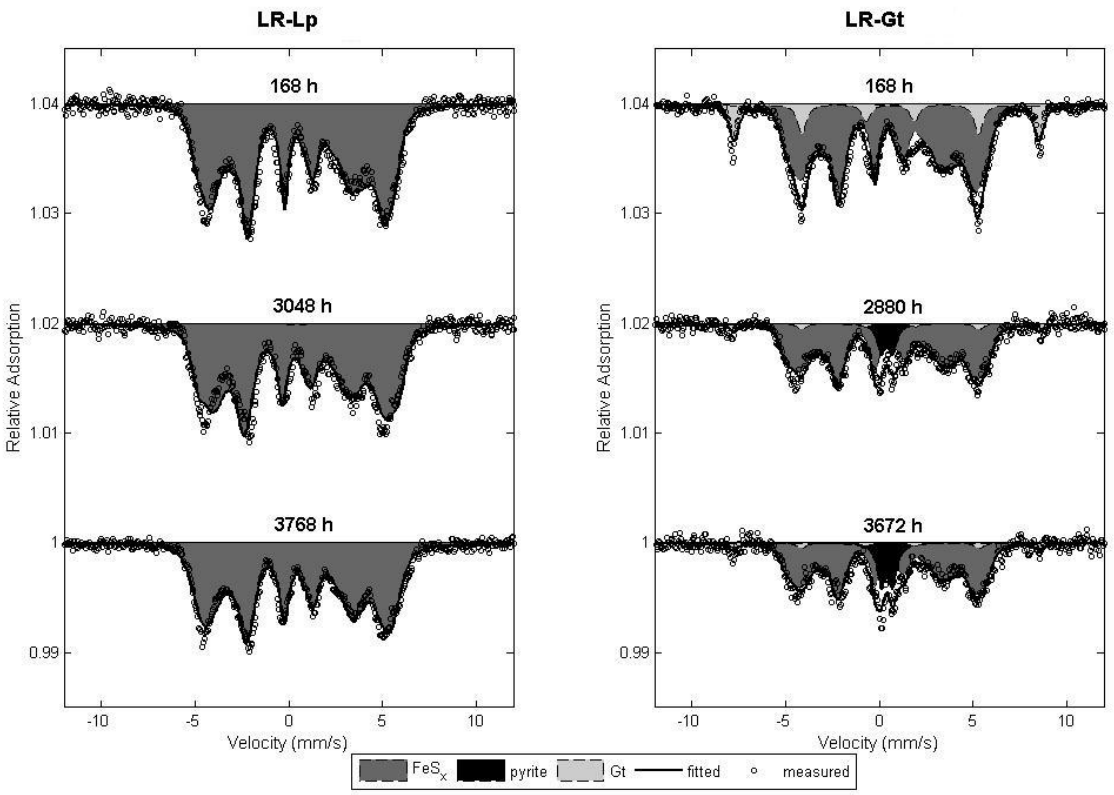

Fig. 6 Mössbauer spectra taken during two long-term LR runs (run 42 and 18) in the presence of high residual aqueous sulfide concentration. The model parameters used for spectra fitting are listed in Table 2.

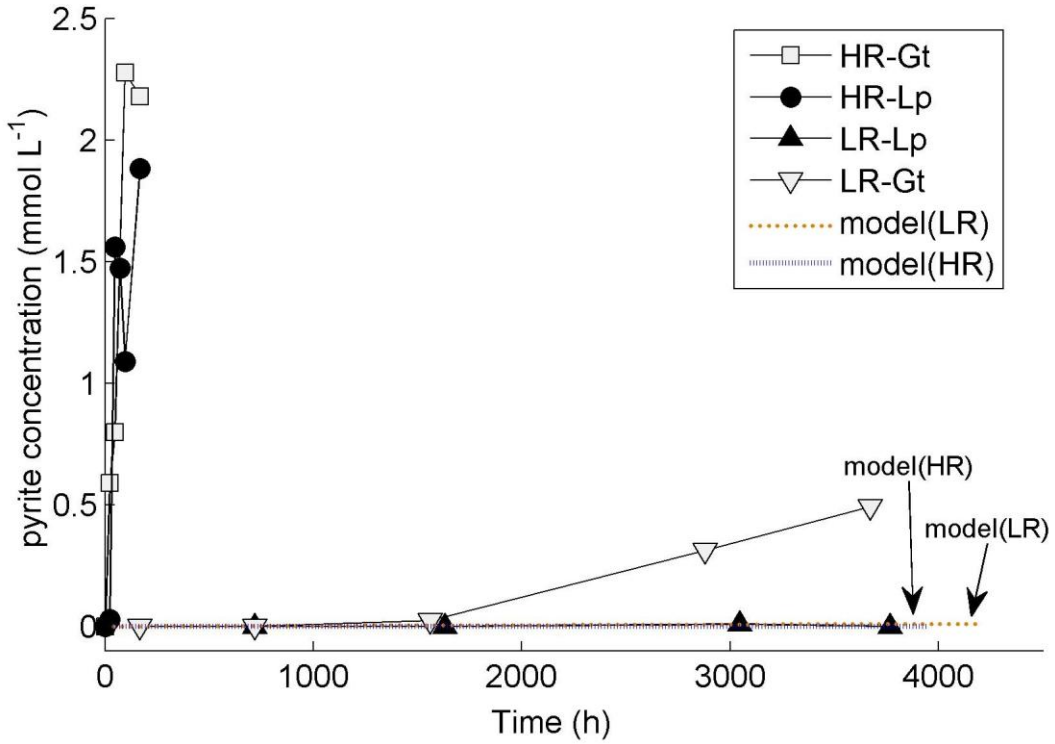

Fig. 7. Temporal change of pyrite concentrations in various HR and LR runs. In the plot, measurements from corresponding runs are lumped together: runs 10 and 11 (HR-Gt), runs 28-30 (HR-Lp), run 42 (LR-Lp), run 18 (LR-Gt). Pyrite concentrations were calculated from data collected by Mössbauer spectroscopy (cf. Table S1 in the Supporting Information). The observed pyrite formation rates in our experiments are distinctly faster than those predicted using Rickard's model (Rickard, 1975) (straight lines) except in the LR-Lp run 42 with high initial sulfide concentration ($S(II)_{aq}$ = 17.4 mmol L^{-1}).

Table 1. Initial conditions for all runs. pH was maintained at 7.0±0.1

Run ID	Name	Runtime	$c(Fe_{tot})$	c(S(-II))	$c(Fe_{tot})$:c(S(-II))
		h	mmol L^{-1}		ratio
1	HR_Gt	3	40.0	7.9	5.1
3	HR_Gt	3	41.7	6.6	6.3
4	HR_Gt	3	39.2	4.4	9.0
5	HR_Gt	3	39.1	6.0	6.5
6	HR_Gt	168	38.6	10.6	3.6
7	HR_Gt	168	35.8	9.6	3.7
9	HR_Gt[a]	168	39.1	8.3	4.7
10	HR_Gt[b]	168	41.6	8.1	5.1
11	HR_Gt[b]	168	39.1	9.7	4.0
14	LR_Gt	216	3.1	8.3	0.4
15	LR_Gt	3600	3.8	13.9	0.3
16	LR_Gt	3600	4.0	14.2	0.3
17	LR_Gt	3600	4.0	14.9	0.3
18	LR_Gt[b]	3600	3.4	14.9	0.2
23	HR_Lp	2.4	22.5	8.0	2.8
24	HR_Lp	264	25.0	7.2	3.5
25	HR_Lp	168	22.1	8.9	2.5
28	HR_Lp[b]	168	15.8	8.0	2.0
29	HR_Lp[b]	48	15.8	7.9	2.0
30	HR_Lp[b]	96	19.2	8.8	2.2
32	LR_Lp	168	4.3	8.2	0.5
33	LR_Lp	168	4.4	8.1	0.5
34	LR_Lp	168	4.2	7.4	0.6
39	LR_Lp	3768	4.1	17.2	0.2
40	LR_Lp	3768	3.5	16.5	0.2
41	LR_Lp	3768	3.4	20.3	0.2
42	LR_Lp[b]	3768	3.8	17.4	0.2

[a] higher temperature (approx. 33°C) at the end of experiment

[b] ^{57}Fe-enriched ferric hydroxides were used, mineral phases in these runs were characterized by Mössbauer spectroscopy

Table 2 Model parameters for Mössbauer spectra of ^{57}Fe hydroxides reacted with sulfide. Spectra were collected at 4.2 K.

	Δ (mm/s)	ΔE_Q (mm/s)	H (T)
Lepidocrocite	0.49	0.03	43.5
Goethite	0.48	-0.11	50.5
FeS_x	0.48	-0.02	27.8
Greigite tetra	0.37	0	30.4
Greigite oct	0.71	-0.015	32.0
pyrite	0.42	0.60	

Table 3 Saturation state of pyrite in representative runs after first reaction phase using aqueous iron and disulfide species

Run		Time	Fe(II)aq	S_n^{2-}(aq)	S_2^{2-} (aq)	Ω_{py}
		h		mmol L^{-1}		
7	HR-Gt	4	0.01	0	0.001 [a]	1.2×10^{14}
25	HR-Lp	3	0.14	0	0.001[a]	1.6×10^{15}
14	LR-Gt	168	0.001[a]	0.2	0.2	2.3×10^{15}
33	LR-Lp	168	0.001[a]	0.2	0.2	2.3×10^{15}

[a] concentration under detection limit. Values based on estimates discussed in the text